JOURNAL OF SOLID STATE CHEMISTRY 81, 173–180 (1989)

Quasi-Two-Dimensional Electronic Properties of the Monophosphate Tungsten Bronzes $Na_xP_4W_8O_{32}$ and $Na_xP_4W_{12}O_{44}$: Crystal Growth, Physical Properties, and Electronic Band Structure

ENOCH WANG AND MARTHA GREENBLATT*

Department of Chemistry, Rutgers The State University of New Jersey, New Brunswick, New Jersey 08903

IDRIS EL-IDRISSI RACHIDI AND ENRIC CANADELL*

Laboratoire de Chimie Theorique, Université de Paris-Sud, 91405 Orsay, France

AND MYUNG-HWAN WHANGBO*

Department of Chemistry, North Carolina State University, Raleigh, North Carolina 27695-8204

Received January 30, 1989

Sodium monophosphate tungsten bronzes $Na_{1.6}P_4W_8O_{32}$ and $Na_2P_4W_{12}O_{44}$ were synthesized, and electrical resistivities and magnetic susceptibilities were measured. These bronzes were found to be quasi-two-dimensional metals and to exhibit weak anomalies in their electrical resistivity and magnetic susceptibility. The possible origin of these anomalies was examined in terms of the tight-binding band electronic structures calculated for the W_4O_{16} and W_6O_{22} slabs of $Na_{1.6}P_4W_8O_{32}$ and $Na_2P_4W_{12}O_{44}$, respectively.

Introduction

Recent studies on the physical properties of tungsten bronzes have yielded interesting correlations between their electronic properties and crystal structure. $CsP_8W_8O_{40}$ (*1*, *2*) is a quasi-one-dimensional (1D) conductor, $K_2P_8W_{24}O_{88}$ (*3*, *4*) and $P_4W_{12}O_{44}$ (*5*, *6*) are quasi-two-dimensional (2D) metals, and $P_8W_{12}O_{52}$ (*7*, *8*) is a three-dimensional (3D) metal. Interesting metal-to-semiconductor and metal-to-metal transitions are observed in the $CsP_8W_8O_{40}$ (*2*) and $P_4W_{12}O_{44}$ (*6*) bronzes, respectively.

$P_4W_{12}O_{44}$ contains ReO_3-type slabs of corner-sharing WO_6 octahedra, which terminate with PO_4 tetrahedra on either side thereby forming pentagonal tunnels at the junction between the slabs (see Fig. 1a). Thus $P_4W_{12}O_{44}$ belongs to the family of the monophosphate tungsten bronzes with pentagonal channels ($MPTB_p$), $(PO_2)_4(WO_3)_{2m}$. Incorporation of alkali metals into monophosphate tungsten bronzes (MPTB) leads to the MPTB's with hexagonal tunnels (i.e., $MPTB_h$), $A_x(PO_2)_4(WO_3)_{2m}$ (*9–14*) (see Fig. 1b).

* Authors to whom correspondence may be addressed.

0022-4596/89 $3.00

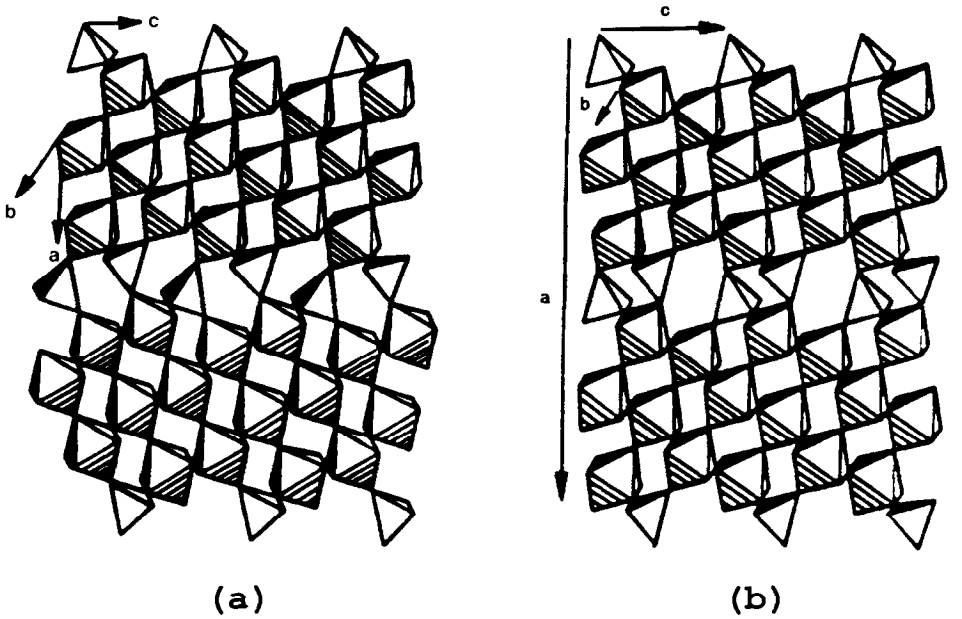

FIG. 1. Schematic representation of the crystal structures of (a) $MPTB_p$ and (b) $MPTB_h$.

Thus the $MPTB_h$'s differ from the $MPTB_p$'s essentially in how their ReO_3-type slabs, W_mO_{3m+4}, are joined together via PO_4 tetrahedra. To a first approximation, the *d*-block band electronic structure of the $MPTB_h$'s and $MPTB_p$'s would be similar except for the number of electrons present in those bands. Therefore, it is interesting to investigate whether or not certain $MPTB_h$'s would exhibit such electronic instabilities as found for the $MPTB_p$, $P_4W_{12}O_{44}$ (*6*). In the present work, we synthesize two $MPTB_h$'s, i.e., $Na_xP_4W_8O_{32}$ and $Na_xP_4W_{12}O_{44}$, measure their electrical resistivities and magnetic susceptibilities, and determine their electronic structures by performing tight-binding band calculations on the W_4O_{16} and W_6O_{22} slabs.

Experimental

A stoichiometric mixture of Na_2CO_3, $(NH_4)_2HPO_4$, and WO_3 needed for $Na_xP_4W_{12}O_{44}$ ($x = 2, 3$) was first heated in air at ~650°C to decompose the phosphate and the carbonate. An adequate amount of metallic W was then added to the initially decomposed product. The final mixture was pelletized and heated to 940°C in an evacuated quartz tube for 3 days and annealed to room temperature in ~7 days. Only polycrystalline samples were obtained by this method. The large single crystals of $Na_2P_4W_{12}O_{44}$ used in characterizing the electronic properties were obtained by reheating a pelletized polycrystalline sample of $Na_2P_4W_{12}O_{44}$ in an evacuated quartz tube at ~1050°C for ~1 week and then slowly cooling it to room temperature in ~2 weeks. Large single crystals of $Na_xP_4W_8O_{32}$ ($x = 1.3, 1.6$) used in the resistivity measurement were obtained during an attempt to synthesize the Na-rich diphosphate tungsten bronze (DPTB), $Na_2P_8W_{12}O_{52}$ (*8*) bronze. A charge appropriate for the nominal composition, $Na_2P_8W_{12}O_{52}$, was heated in an evacuated quartz tube at ~1050°C for ~2 weeks before annealing slowly to room temperature in ~2 weeks.

Substitutional or extraction reactions of Na in $Na_xP_4W_8O_{32}$ ($x = 2, 3$) were carried out by excess sulfur, I_2, KBr, KI, and RbI at 900°C for ~5 days and followed by cooling to room temperature in ~1 week. All phases were identified by powder X-ray diffraction using a Scintag PAD V system with monochromatized Cu$K\alpha$ radiation and Si as an internal standard.

Standard, four-probe, low-temperature (2–270 K) dc resistivity measurements were made on oriented single crystals of $Na_2P_4W_{12}O_{44}$ and $Na_{1.6}P_4W_8O_{32}$. Crystal orientations were determined by precession techniques. Electrical contacts were made with ultrasonically evaporated indium. Magnetic susceptibility on single crystals was measured on a Quantum Design SQUID magnetometer between 3 and 290 K. Elemental analysis was performed with a Beckmann plasma emission spectrometer.

Tight-binding band electronic structure calculations (*15*) were carried out on the W_4O_{16} and W_6O_{22} slabs within the framework of the extended Hückel method (*16*).[1] The atomic parameters employed in our work were taken from the previous work (*2b*).

Results and Discussion

Synthesis

Purple, plate-like crystals of $Na_2P_4W_{12}O_{44}$ (Fig. 2) were obtained in the hot zone. The largest crystals have dimensions of ~6 × 3 × 0.8 mm^3. These purple crystals appear to be dichromic with golden edges. The monoclinic ($P2_1/a$) unit cell parameters of $Na_2P_4W_{12}O_{44}$, $a = 23.765(4)$, $b = 5.2837(9)$, $c = 6.580(1)$ Å, and $\beta = 93.44(1)°$ as determined by least-squares fitting of the observed powder X-ray diffraction data are in good agreement with those previously reported for $Na_xP_4W_{12}O_{44}$ by Raveau *et al.* (*9*). For $Na_xP_4W_8O_{32}$, copper-colored, plate-like crystals with an average size of 4 × 1.5 × 0.8 mm^3 were obtained in both the hot and cold zones of a quartz ampoule containing a charge of the composition $Na_2P_8W_{12}O_{52}$. The hot zone grown crystals have a better morphology than the cold zone ones. The unit cell parameters of monoclinic $Na_xP_4W_8O_{32}$ (space group $P2_1/a$) are: $a = 17.788(6)$, $b = 5.284(1)$, $c = 6.608(3)$ Å, and $\beta = 99.7(3)°$, in excellent agreement with previously reported results for $Na_xP_4W_8O_{32}$ (*9*).

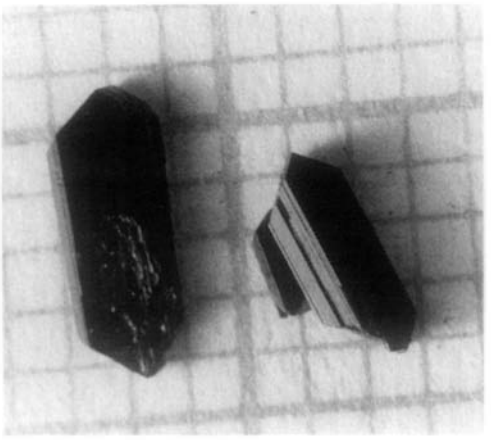

FIG. 2. $Na_2P_4W_{12}O_{44}$ crystals.

Attempts to remove Na from $Na_2P_4W_{12}O_{44}$ resulted in mixed phases which exhibit the $P_4W_{12}O_{44}$ ($MPTB_p$) and $Na_xP_4W_{12}O_{44}$ ($MPTB_h$) structures. Although the overall composition of the two phases is $Na_{0.9}P_4W_{12}O_{44}$, the actual compositions of the two phases are probably $Na_xP_4W_{12}O_{44}$ ($x > 1$, $MPTB_h$) and $Na_xP_4W_{12}O_{44}$ ($x \leq 1$, $MPTB_p$). This is supported by previous unsuccessful attempts to synthesize the $MPTB_h$ structure of $NaP_4W_{12}O_{44}$; $NaP_4W_{12}O_{44}$ with $MPTB_p$ structure was obtained instead. Thus, in $Na_x(PO_2)_4(WO_3)_{2m}$, $x > 1$ is needed to obtain the $MPTB_h$ phase and the $MPTB_p$

[1] A modified Wolfsberg-Helmholz formula was used to calculate the off-diagonal H_{ij} values. See Ref. (*17*).

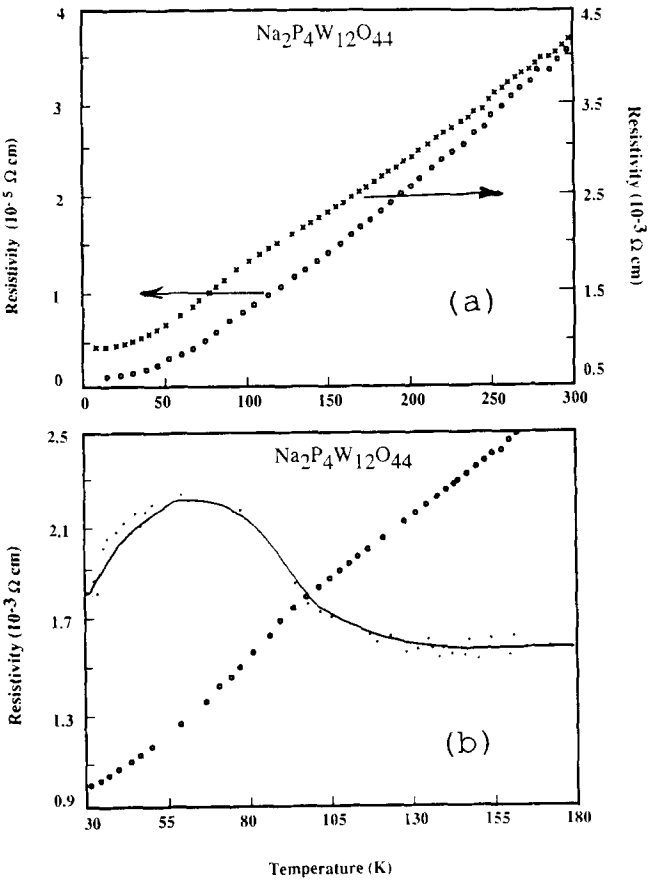

FIG. 3. (a) Temperature-dependent resistivities of $Na_2P_4W_{12}O_{44}$ along b (○) and a^* (x). (b) Enlarged view of the resistivity transition (○) and its $d\rho/dT$ plot (·).

phase will be the stable phase if $x \leq 1$. Similar phase boundary also exists in the $K_x(PO_2)_4(WO_3)_{2m}$ ($MPTB_h$) bronzes where it has been reported (*12*) that the $MPTB_h$ and $DPTB_h$ phases are stable for $x < \sim 1$ and $x > \sim 1$, respectively. Thus, when Na is partially substituted by K, a $DPTB_h$-type phase with the composition $K_{1.03}Na_{0.53}P_4W_{12}O_{44}$ is obtained. Rb does not substitute for Na in $Na_3P_4W_{12}O_{44}$ probably because it is too big to occupy the Na sites in the tunnels. Thus, the $MPTB_h$ structure of $Na_x(PO_2)_4(WO_3)_{2m}$ is a suitable candidate for the study of the relationship between structure vs alkali ion content. The $MPTB_h$ structure may be considered as the intermediate phase between the $MPTB_p$ and $DPTB_h$ phases.

Electrical Resistivity and Magnetic Susceptibility

Room-temperature resistivities of a single crystal of $Na_2P_4W_{12}O_{44}$ along the three crystallographic directions are indicative of a quasi-2D metal; $\rho_{a^*} = 4.2 \times 10^{-3}$ Ω cm, $\rho_b = 3.4 \times 10^{-5}$ Ω cm, and $\rho_{c^*} = 8.3 \times 10^{-5}$ Ω cm. Similar results were obtained for $Na_{1.6}P_4W_8O_{32}$: $\rho_{a^*} = 5.0 \times 10^{-4}$ Ω cm, $\rho_b = 1.2 \times 10^{-5}$ Ω cm, and $\rho_{c^*} = 7.6 \times 10^{-5}$ Ω cm. In both cases, the resistivity along b is slightly lower than that along c^*. However, the

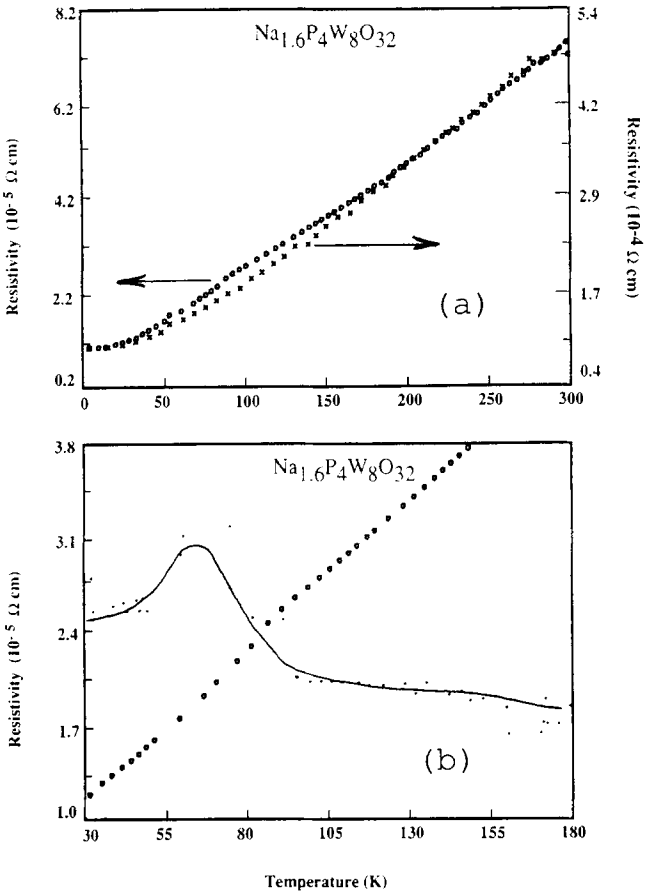

FIG. 4. (a) Temperature-dependent resistivities of $Na_{1.6}P_4W_8O_{32}$ along b (○) and a^* (x). (b) Enlarged view of the resistivity transition (○) and its dp/dT plot (·).

anisotropy between the easy directions (i.e., $\parallel b$ or $\parallel c^*$) and the hard direction (i.e., $\parallel a^*$) is one order of magnitude larger in $Na_2P_4W_{12}O_{44}$ than in $Na_{1.6}P_4W_8O_{32}$ bronzes. Temperature dependent resistivities of both $Na_2P_4W_{12}O_{44}$ (Fig. 3) and $Na_{1.6}P_4W_8O_{32}$ (Fig. 4) bronzes reveal metallic behavior. A weak and broad metal-to-metal transition is observed at ~140 K both along a^* and b in $Na_2P_4W_{12}O_{44}$. In $Na_{1.6}P_4W_8O_{32}$, the metal-to-metal transition is weaker but observable at ~90 K along b. The onset temperatures of these weak transitions cannot be determined accurately from the ρ vs T plots.

Magnetic susceptibility of $Na_2P_4W_{12}O_{44}$ (Fig. 5) is Pauli paramagnetic from room temperature to ~150 K where a downturn in χ is observed, corresponding approximately to the transition seen in the resistivity measurement. In $Na_{1.6}P_4W_8O_{32}$, the transition seen at ~100 K in the magnetic susceptibility (Fig. 6) corresponds to the anomaly seen at ~90 K in the resistivity.

Band Electronic Structures

Figures 7a and 7b show the dispersion relations of the bottom portion of the t_{2g}-block bands calculated for $Na_{1.6}P_4W_8O_{32}$ and $Na_2P_4W_{12}O_{44}$, respectively, where the

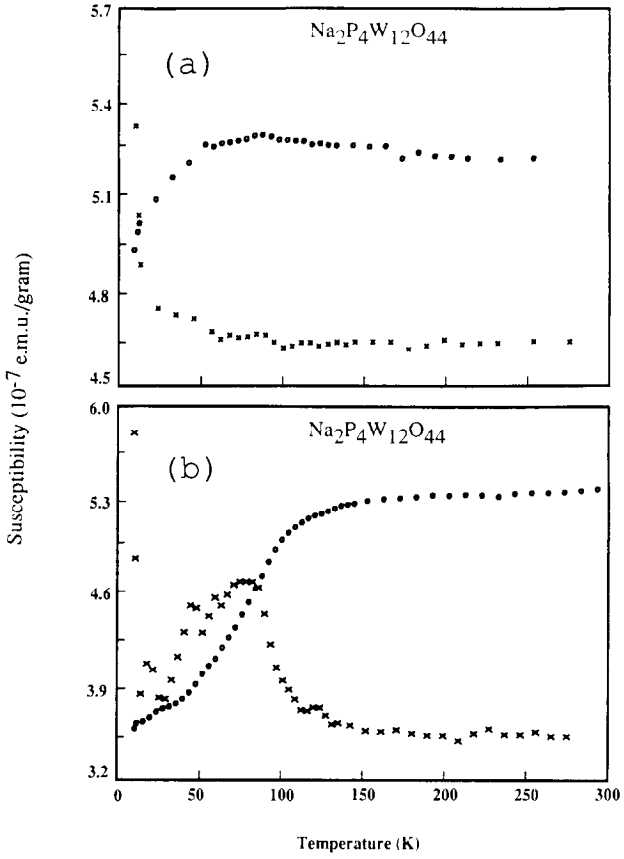

FIG. 5. (a) χ vs T (○) and $d\chi/dT$ (x) of $Na_2P_4W_{12}O_{44}$, with H in the bc plane (easy direction). (b) χ vs T (○) and $d\chi/dT$ (x) with $H \parallel a^*$ (hard direction).

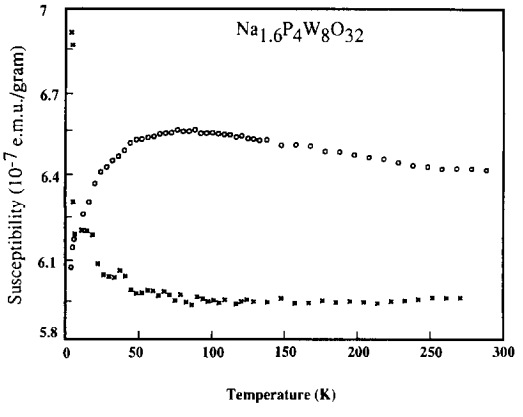

FIG. 6. χ vs T (○) and $d\chi/dT$ (x) of a batch of randomly oriented crystals of $Na_{1.6}P_4W_8O_{32}$.

dashed lines refer to the Fermi levels. Essentially, the two band structures are similar, and the bottom three bands of either Fig. 7a or Fig. 7b can be considered in terms of one 1D and two 2D bands (*18*). Those bands are cut by the Fermi level, and their Fermi surfaces calculated from $Na_{1.6}P_4W_8O_{32}$ and $Na_2P_4W_{12}O_{44}$ are shown in Figs. 8 and 9, respectively, where the wave vectors of the shaded regions give rise to the filled band levels. Note that, in Figs. 8a and 9a, the Fermi surfaces arising from the bottom two bands are combined together in an extended zone scheme.

Figures 8a and 9a both consist of 1D and 2D Fermi surfaces, while Figs. 8b and 9b

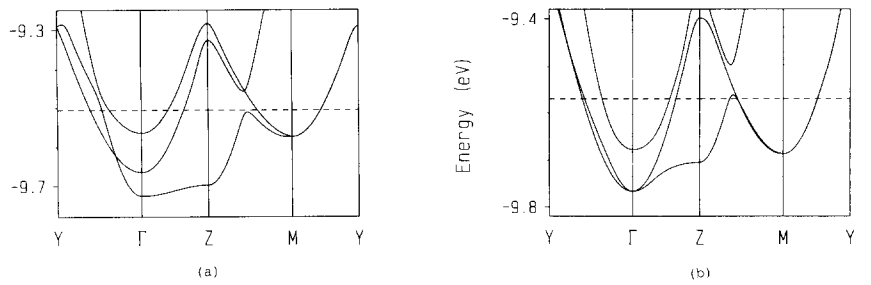

FIG. 7. Dispersion relations of the bottom portion of the t_{2g}-block bands calculated for (a) the W_4O_{16} slab of $Na_{1.6}P_4W_8O_{32}$ and (b) the W_6O_{22} slab of $Na_2P_4W_{12}O_{44}$. Here $\Gamma = (0, 0)$; $Y = (b^*/2, 0)$; $Z = (0, c^*/2)$; and $M = (b^*/2, c^*/2)$.

both consist of a 2D Fermi surface. Since the 1D Fermi surface is open along the $\Gamma \rightarrow Z$ direction, it is expected that the electrical conductivities of $Na_{1.6}P_4W_8O_{32}$ and $Na_2P_4W_{12}O_{44}$ will be greater along the crystallographic b-axis than along the c-axis. This expectation is in good agreement with our observation.

The 1D and 2D Fermi surfaces of Figs. 8 and 9 have flat portions, which can provide nesting and therefore lead to instabilities. Such electronic instabilities may be responsible for the weak resistivity anomalies seen for $Na_{1.6}P_4W_8O_{32}$ and $Na_2P_4W_{12}O_{44}$. The resistivity anomalies of the $MPTB_p$, $P_4W_{12}O_{44}$, which are believed to arise from CDW instabilities (*6*), are much stronger than those of $Na_{1.6}P_4W_8O_{32}$ and $Na_2P_4W_{12}O_{44}$. The weak resistivity anomalies of the latter, if caused by CDW instabilities as suggested above, might originate from the random potentials generated by the disordered distribution of Na ions in the hexagonal channels. In principle, it is possible that the weak resistivity anomalies may have a nonelectronic origin. Further studies are needed to clarify the nature of the weak resistivity anomalies of $Na_{1.6}P_4W_8O_{32}$ and $Na_2P_4W_{12}O_{44}$.

Concluding Remarks

The electrical resistivities of $Na_{1.6}P_4W_8O_{32}$ and $Na_2P_4W_{12}O_{44}$ show that these bronzes are 2D metals with the best electrical conductivity along the b-axis. Our band electronic structure calculations are in accord with this observation. Both the electrical resistivities and the magnetic susceptibilities of $Na_{1.6}P_4W_8O_{32}$ and $Na_2P_4W_{12}O_{44}$

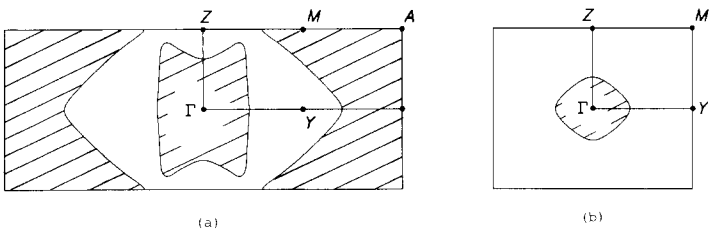

FIG. 8. Fermi surfaces associated with the bottom three d-block bands of Fig. 7a: (a) the Fermi surfaces of the two lowest lying bands combined together in an extended zone scheme, where $A = (b^*, c^*/2)$, and (b) the Fermi surface of the highest lying band of the three.

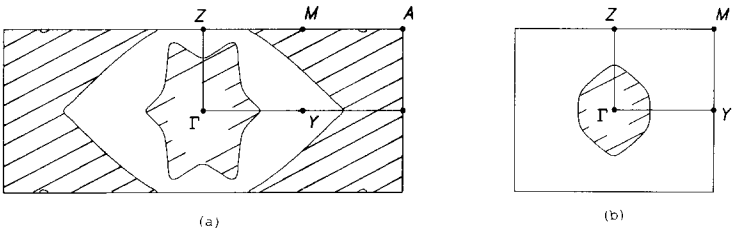

FIG. 9. Fermi surfaces associated with the bottom three *d*-block bands of Fig. 7b: (a) the Fermi surfaces of the two lowest lying bands combined together in an extended zone scheme, and (b) the Fermi surface of the highest lying band of the three.

exhibit weak anomalies at ~90 and ~140 K, respectively. Our band electronic structure calculations suggest that those weak anomalies may be associated with CDW instabilities arising from partial Fermi surface nesting. However, we could not exclude other nonelectronic origin for the weak anomalies.

Acknowledgments

Work at Rutgers University was supported by the National Science Foundation–Solid State Chemistry Grants DMR-84-04003 and DMR-87-14072 and by the National Science Foundation Materials Research Instrumentation Grants DMR-84-08266 and DMR-87-05620. Work at Université de Paris-Sud and North Carolina State University was supported by NATO, Scientific Affairs Division, and also by DOE, Office of Basic Energy Sciences, Division of Materials Sciences, under Grant DE-FG05-86ER45259.

References

1. M. GOREAUD, PH. LABBE, AND B. RAVEAU, *J. Solid State Chem.* **56,** 41 (1985).
2. (*a*) E. WANG AND M. GREENBLATT, *J. Solid State Chem.* **76,** 340 (1988); (*b*) E. WANG, M. GREENBLATT, I. E.-I. RACHIDI, E. CANADELL, AND M.-H. WHANGBO, *Inorg. Chem.*, in press.
3. E. WANG, M. GREENBLATT, I. E.-I. RACHIDI, E. CANADELL, AND M.-H. WHANGBO, *J. Solid State Chem.*, in press.
4. J. P. GIROULT, M. GOREAUD, PH. LABBE, AND B. RAVEAU, *Acta. Crystallogr. Sect. B* **37,** 1163 (1981).
5. PH. LABBE, M. GOREAUD, AND B. RAVEAU, *J. Solid State Chem.* **61,** 324 (1986).
6. E. WANG, M. GREENBLATT, I. E.-I. RACHIDI, E. CANADELL, AND M.-H. WHANGBO, *Phys. Rev. B*, in press.
7. B. DOMENGES, M. GOREAUD, PH. LABBE, AND B. RAVEAU, *Acta Crystallogr. Sect. B* **38,** 1724 (1982).
8. E. CANADELL, I. E.-I. RACHIDI, E. WANG, M. GREENBLATT, AND M.-H. WHANGBO, *Inorg. Chem.*, in press.
9. A. BENMOUSSA, D. GROULT, PH. LABBE, AND B. RAVEAU, *Acta Crystallogr. Sect. C* **40,** 573 (1984).
10. M. LAMIRE, PH. LABBE, M. GOREAUD, AND B. RAVEAU, *J. Solid State Chem.* **66,** 64 (1987).
11. J. P. GIROULT, M. GOREAUD, PH. LABBE, AND B. RAVEAU, *J. Solid State Chem.* **44,** 407 (1982).
12. B. DOMENGES, M. HERVIEU, B. RAVEAU, AND M. O'KEEFFE, *J. Solid State Chem.* **72,** 155 (1988).
13. B. DOMENGES, M. GOREAUD, PH. LABBE, AND B. RAVEAU, *J. Solid State Chem.* **50,** 173 (1983).
14. A. BENMOUSSA, D. GROULT, AND B. RAVEAU, *Rev. Chim. Miner.* **21,** 710 (1984).
15. M.-H. WHANGBO AND R. HOFFMANN, *J. Amer. Chem. Soc.* **100,** 6093 (1978).
16. R. HOFFMANN, *J. Chem. Phys.* **39,** 1397 (1963).
17. J. H. AMMETER, H.-B. BÜRGI, J. THIBEAULT, AND R. HOFFMANN, *J. Amer. Chem. Soc.* **100,** 2686 (1978).
18. I. E.-I. RACHIDI, E. CANADELL, AND M.-H. WHANGBO, to be published.